THE JOURNAL OF BIOLOGICAL CHEMISTRY VOL. 282, NO. 44, pp. 32144–32151, November 2, 2007

Identification of the MxiH Needle Protein Residues Responsible for Anchoring Invasion Plasmid Antigen D to the Type III Secretion Needle Tip*[S]

Received for publication, April 24, 2007, and in revised form, September 5, 2007 Published, JBC Papers in Press, September 7, 2007, DOI 10.1074/jbc.M703403200

Lingling Zhang, Yu Wang, Andrew J. Olive, Nathan D. Smith, William D. Picking, Roberto N. De Guzman, and Wendy L. Picking[1]

From the Department of Molecular Biosciences, University of Kansas, Lawrence, Kansas 66045

The pathogenesis of *Shigella flexneri* requires a functional type III secretion apparatus to serve as a conduit for injecting host-altering effector proteins into the membrane and cytoplasm of the targeted cell. The type III secretion apparatus is composed of a basal body and an exposed needle that is an extended polymer of MxiH with a 2.0-nm inner channel. Invasion plasmid antigen D (IpaD) resides at the tip of the needle to control type III secretion. The atomic structures of MxiH and IpaD have been solved. MxiH (8.3 kDa) is a helix-turn-helix, whereas IpaD (36.6 kDa) has a dumbbell shape with two globular domains flanking a central coiled-coil that stabilizes the protein. These structures alone, however, have not been sufficient to produce a workable *in silico* model by which IpaD docks at the needle tip. Thus, the work presented here provides an initial step in understanding this important protein-protein interaction. We have identified key MxiH residues located in its PSNP loop and the contiguous surface that uniquely contribute to the formation of the IpaD-needle interface as determined by NMR chemical shift mapping. Mutation of Asn-43, Leu-47, and Tyr-50 residues severely affects the stable maintenance of IpaD at the *Shigella* surface and thus compromises the invasive phenotype of *S. flexneri*. Other residues could be mutated to give rise to intermediate phenotypes, suggesting they have a role in tip complex stabilization while not being essential for tip complex formation. Initial *in vitro* fluorescence polarization studies confirmed that specific amino acid changes adversely affect the MxiH-IpaD interaction. Meanwhile, none of the mutations appeared to have a negative effect on the MxiH-MxiH interactions required for efficient needle assembly.

Shigella flexneri is a Gram-negative bacterium and the causative agent of shigellosis, a potentially life-threatening form of bacillary dysentery. Although shigellosis is often considered a disease restricted to the developing world, it is also a problem in industrialized nations as an infectious agent in daycare centers, nursing homes, and situations where public health infrastructure becomes compromised (1). The problems posed by shigellosis are compounded by increasing numbers of antibiotic-resistant isolates and the need to send aid personnel to endemic areas (2).

Once ingested, *Shigella* passes through the stomach to the colonic mucosa where it crosses M cells into gut-associated lymphoid tissues (3). The bacterium then enters macrophages and induces them to undergo apoptosis (4), which leads to release of the pathogen at the basolateral side of the colonic epithelium. *Shigella* then promotes its own uptake into epithelial cells by inducing cytoskeletal rearrangements in these cells (5, 6). The pathogenesis of *S. flexneri* requires a functional type III secretion system (6). Type III secretion systems are a shared virulence determinant for many Gram-negative animal and plant pathogens, and they are used to deliver protein effectors to targeted cells to subvert normal cellular functions (7, 8). The type III secretion apparatus (TTSA)[2] visually resembles a molecular needle and syringe (9, 10). It is composed of a basal body that spans both bacterial membranes and an exposed needle that is a polymer of MxiH. The needle is ~50 nm in length, has an outer diameter of 7.0 nm, and possesses an inner channel that is ~2.0–3.0 nm in diameter (10, 11). We recently demonstrated that invasion plasmid antigen D (IpaD) localizes to the tip of the TTSA needle (12), where it controls secretion of the translocator proteins IpaB and IpaC and directs their insertion into host cell membranes (13). From its position at the TTSA needle tip, IpaD is responsible for recruiting and stably maintaining IpaB to this site in the presence of bile salts (14). This is an essential step for *Shigella* invasiveness, and the interactions between IpaD and MxiH that are responsible for tip complex stabilization are thus critical for *Shigella* pathogenesis (12, 14).

The high resolution structures of MxiH and IpaD were recently reported (15, 16). MxiH monomers possess a helix-turn-helix head group with an elongated C-terminal helix (15). The head group is stabilized by hydrophobic contacts of residues at the interface between the two helices that flank a central PSNP loop (15). Likewise, the TTSA needle appears to pack by

* This work was supported by Public Health Service Grants AI034428 and AI057927 (to W. D. P.), AI067858 (to W. L. P.), and RR017708 (CoBRE Protein Structure and Function Program) and Kansas University start-up funds (to R. N. D.). The costs of publication of this article were defrayed in part by the payment of page charges. This article must therefore be hereby marked "*advertisement*" in accordance with 18 U.S.C. Section 1734 solely to indicate this fact.

The chemical shift assignments for MxiH$^{C\Delta5}$ have been deposited at the Biological Magnetic Resonance Bank (BMRB accession number 15214).

[S] The on-line version of this article (available at http://www.jbc.org) contains supplemental Figs. S1–S3 and Table S1.

[1] To whom correspondence should be addressed: Dept. of Molecular Biosciences, University of Kansas, 1200 Sunnyside Ave., Lawrence, KS 66045-7534. Tel.: 785-864-3299; Fax: 785-864-5294; E-mail: pickingw@ku.edu.

[2] The abbreviations used are: TTSA, type III secretion apparatus; FM, fluorescein maleimide; FP, fluorescence polarization; mP, millipolarization; IpaD, invasion plasmid antigen D.

polar contacts between the individual MxiH monomers with the PSNP loop facing outward and upward relative to the central channel (15). In contrast to MxiH, IpaD has a more complex structure that gives it a dumbbell shape (16). IpaD has a central coiled-coil that defines the handle of the dumbbell and is flanked at each end by distinct N- and C-terminal domains (16). This shape defines the tip proteins as a unique class (17) and appears to be important for IpaD localization at the tip of the needle (12). Based on *in silico* modeling of the *Yersinia* tip complex protein LcrV on the *Shigella* MxiH needle tip, the LcrV N-terminal globular domain and the C-terminal end of the coiled-coil are both required in docking LcrV on the needle (15). Although the IpaD structure shows that the N-terminal domain can mimic a MxiH molecule and possibly serve to chaperone the C-terminal coil to prevent the binding of MxiH and IpaD in the cytoplasm, how IpaD docks to MxiH could not be resolved even after the structure of the two proteins became available (16). Nevertheless, interactions in addition to those that dictate needle assembly would be expected to be involved in maintaining IpaD at the needle tip. We therefore chose to examine the structural basis for the interaction between MxiH and IpaD. The data presented here show that specific residues within the MxiH head group are located at the MxiH-IpaD interface. These residues are needed for stable maintenance of IpaD at the TTSA needle tip but are distinct from those needed for needle assembly.

EXPERIMENTAL PROCEDURES

Materials—Antibodies to MxiH and IpaD were a kind gift from E. V. Oaks (Walter Reed Army Institute for Research, Silver Springs, MD). The *S. flexneri mxiH* null strain SH116 was from A. Allaoui (Brussels, Belgium) and grown at 37 °C in trypticase soy agar containing 0.025% Congo red to ensure the presence of the virulence plasmid. Sheep red blood cells were from Colorado Serum Company (Denver, CO). Fluorescent probes and Alexa Fluor-labeled secondary antibodies were from Molecular Probes (Eugene, OR). *Escherichia coli* Tuner(DE3), pET15b, pET22b, and ligation reagents were from Novagen (Madison, WI). Restriction enzymes were from New England Biolabs (Tozer, MA). Oligonucleotide primers were from IDT (Coralville, IA). ^{15}N-Ammonium chloride and $^{13}C_6$-glucose were from Cambridge Isotope Laboratories, Inc. (Andover, MA). Iminodiacetic acid affinity resin was from Sigma. Other chemicals were reagent grade.

Protein Expression and Purification—Recombinant IpaD was prepared by standard methods as previously described (18). The mxiHΔ5/pET22b was subcloned from pRKmxiH$^{C\Delta5}$ (19, 20). This was the construct used to solve the crystal structure of MxiH$^{C\Delta5}$ (15). To maintain MxiH in monomeric form, five codons have been deleted from the 3′-end of the *mxiH* coding sequence, *mxiH*$^{C\Delta5}$, giving rise to MxiH$^{C\Delta5}$. This mutation also prevents polymerization of needles *in vivo*, resulting in secretion of MxiH$^{C\Delta5}$ monomers but a phenotype that is otherwise like a *mxiH* null mutant (19). To obtain uniformly ^{15}N,^{13}C-labeled MxiH$^{C\Delta5}$, mxiHΔ5/pET22b in *E. coli* Tuner(DE3) was grown in minimal medium supplemented with ^{15}N NH_4Cl and ^{13}C-glucose as the sole nitrogen and carbon sources, respectively (21). After reaching mid log phase, bacteria were induced to produce protein with 1 mM isopropyl-1-thio-β-D-galactopyranoside and grown at 15 °C overnight. Bacteria were collected, resuspended in IMAC binding buffer (20 mM Tris·HCl, pH 7.9, 50 mM NaCl, 5 mM imidazole) and sonicated, and the cellular debris was removed by centrifugation. Recombinant protein was purified via His_6 tag by IMAC chromatography as described (20, 22). Fractions were pooled and dialyzed into appropriate buffers (see below), and the protein concentration was estimated by UV absorbance at 280 nm.

NMR Spectroscopy—Uniformly ^{15}N- or ^{15}N,^{13}C-labeled MxiH$^{C\Delta5}$ and unlabeled IpaD were dissolved in NMR buffer (10 mM sodium phosphate, pH 6.0, 10 mM NaCl, 10% D_2O, and 90% H_2O). NMR data were acquired at 25 °C on a Bruker Avance 800 MHz spectrometer fitted with a cryogenic triple-resonance probe and a *Z*-axis pulse field gradient. NMR data were processed using NMRPipe (23) and analyzed using NMRView (24). Backbone resonances of free MxiH$^{C\Delta5}$ were assigned using ^{1}H-^{15}N HSQC, HNCA, CBCA(CO)NH, and HNCACB acquired using a 0.8 mM ^{15}N,^{13}C-MxiH$^{C\Delta5}$ sample as described for BsaL$^{C\Delta5}$ (21). Chemical shift mapping was done by acquiring two-dimensional ^{1}H-^{15}N HSQC at MxiH $^{C\Delta5}$:IpaD molar ratios of 0.5, 1, 2, 4, and 8. Both IpaD and MxiH$^{C\Delta5}$ were dialyzed into the same buffer prior to titration to assure that the chemical shift changes were only due to protein-protein interactions and not to changes in solution condition upon mixing.

Preparation of mxiH Mutants for Expression in S. flexneri SH116—pRKmxiH containing the *mxiH* gene has been described (19). *mxiH* mutants were made by inverse PCR using pRKmxiH as template, a primer composed of GAGAGA, a restriction site, and 18 nucleotides flanking the nucleotides to be deleted and a primer going the opposite direction encoding GAGAGA, a restriction site, and 18 nucleotides (19). The generation of MxiH^{Q51A} has been described (19). The primers used to introduce mutations into MxiH are given in supplemental Table S1. The PCR product was digested with the appropriate restriction enzyme, intramolecularly ligated, and used to transform *E. coli* NovaBlue. Double-stranded sequencing was performed on each new mutant *mxiH* gene to ensure only the desired mutation was incorporated. Each plasmid was electroporated into *S. flexneri* SH116. Ampicillin selection ensured presence of the plasmid while kanamycin resistance and/or Congo red binding indicated the presence of the *Shigella* virulence plasmid.

Phenotypic Characterization of S. flexneri SH116 Expressing Different mxiH Mutants—The phenotype of each newly generated *mxiH* point mutant strain of *Shigella* was determined by standard assays. *Shigella* invasion functions were tested using a gentamycin protection invasion assay with cultured Henle 407 as described (25). Contact-mediated hemolysis with sheep erythrocytes was used to measure the IpaD-dependent insertion of IpaB and IpaC into target cell membranes as described (25). The overnight secretion of Ipa proteins into *Shigella* culture supernatants was used to ascertain the presence of functional TTSAs and, more specifically, the assembly of functional MxiH needles with IpaD at the tip as recently described (12). Induction of type III secretion was tested using Congo red as an artificial inducer of secretion (19). In *S. flexneri*, type III secretion occurs upon host cell contact; however, this event can be mimicked by the addition of Congo red (26). The surface local-

ization of IpaD was determined using immunofluorescence microscopy while the ability to polymerize MxiH needles was determined by transmission electron microscopy as recently described (12, 19).

Preparation of mxiH$^{C\Delta5}$ Mutants for Expression in E. coli Tuner(DE3)—To produce monomeric protein, 5 residues were deleted from the C terminus of MxiH (15). Therefore, the mutant *mxiH$^{C\Delta5}$* genes were copied from the corresponding pLZ plasmid by PCR using a 5′-primer containing GAGAGA, an NdeI restriction site, and the first 18 bases of *mxiH* and a 3′-primer containing GAGAGA, a XhoI restriction site, and the last 18 bases of *mxiH* excluding the stop codon and the last 5 amino acids. The PCR product was digested with NdeI and XhoI and ligated into correspondingly digested pET22b, and the ligated product was transformed into *E. coli* NovaBlue. Double-stranded sequencing was performed on each new mutant *mxiH$^{C\Delta5}$* gene to confirm that only the desired mutation was incorporated. The resulting plasmid was used to transform *E. coli* Tuner(DE3). This strain was used for purification of the mutant MxiH$^{C\Delta5}$ proteins as previously described (22).

Fluorescence Polarization—The interaction of IpaD with MxiH$^{C\Delta5}$ and MxiH$^{C\Delta5}$ mutants was measured by fluorescence polarization (FP) (27). FP provides a measure of the rotational diffusion for a fluorescent molecule in solution. Small molecules rotate quickly, which produces rapid depolarization of the population of fluorescent molecules selected using excitation by polarized light, thus giving rise to low millipolarization (mP) values. In contrast, larger molecules rotate more slowly and display a reduced rate in depolarization in aqueous solution, thereby leading to larger mP values. The association of a small fluorescent species with a larger nonfluorescent species results in a significant increase in overall molecular volume, thus resulting in an increase in the mP of the fluorescent species.

IpaD was labeled with fluorescein at its single Cys residue by combining 1 ml of IpaD (3 mg/ml) in phosphate-buffered saline (pH 7.5) with 50 μl of fluorescein maleimide (FM) prepared as a 1 mg/ml stock prepared in *N*,*N*-dimethylformamide. After incubating the mixture for 1 h at 4 °C, the reaction was stopped by adding dithiothreitol to 1 mM. The FM-IpaD was isolated from the free fluorophore by gel filtration using Sephadex G-50. FP measurements were obtained using a Beacon fluorescence polarimeter (Panvera Corp.) as described (27). Briefly, a constant concentration of FM-IpaD (20 nM) in phosphate-buffered saline was mixed with increasing concentrations of MxiH$^{C\Delta5}$. The change in FP, measured in millipolarization units (ΔmP), was monitored after adding nonfluorescent MxiH$^{C\Delta5}$.

RESULTS AND DISCUSSION

MxiH$^{C\Delta5}$ Binding to IpaD—We recently showed that IpaD localizes to the tip of the TTSA needle (12). Although our findings show that the C-terminal coil of IpaD is responsible for its maintenance at the MxiH needle tip, no such data are available to directly demonstrate the structural role of the TTSA needle protein in the IpaD-MxiH interaction. Using FP to detect *in vitro* protein-protein interactions, a direct interaction between MxiH$^{C\Delta5}$ and IpaD was identified (Fig. 1). IpaD was labeled with FM at Cys-322, which is the only free thiol in IpaD. Cys-322 is 10 residues away from the IpaD C terminus, and it is this

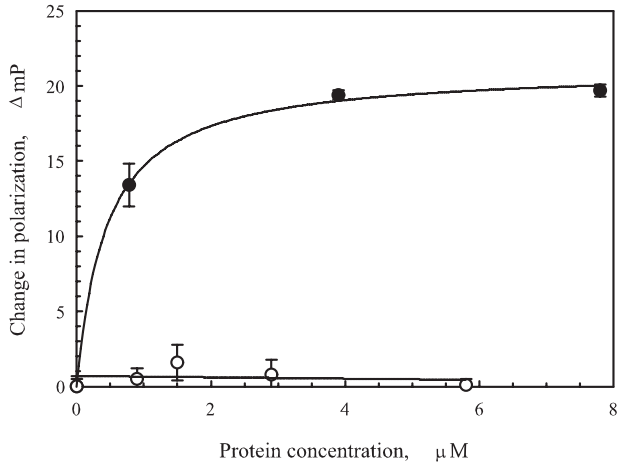

FIGURE 1. **Interaction of IpaD with MxiH.** FM-labeled IpaD (200 nM) was incubated with MxiH$^{C\Delta5}$ (●) or IpgC (○). The change in the polarization value (Δ*mP*) of the FM-IpaD was measured as a function of MxiH concentration. Addition of anti-IpaD IgG resulted in a maximum ΔmP of 30.8 ($n = 3$).

portion of IpaD that mediates its stable association with the *Shigella* TTSA needle tip (12). The initial polarization value for IpaD was 247.9 ± 0.7, a high value that is consistent with the attachment of the probe to a large (36.6-kDa) protein. FM-IpaD association with MxiH$^{C\Delta5}$ resulted in a measured increase of 21.2 mP whereas no change was seen upon the addition of IpgC, the bacterial cytoplasmic type III secretion system translocator chaperone (Fig. 1). Because the maximum ΔmP achieved by the addition of anti-IpaD IgG is 30.8, the change in polarization upon addition of MxiH$^{C\Delta5}$ represents a significant change based on the fact that its mass is only one fourth that of IpaD. The fact that a detectable change is observed most likely stems from the previous observation that IpaD association with the MxiH needle involves the C terminus of IpaD (12) and this is near where the FM labeling occurs. The data presented thus indicate that IpaD and MxiH$^{C\Delta5}$ interactions are detectable *in vitro*. Furthermore, the binding data suggest that the two proteins have an apparent dissociation constant (k_d) of ~0.48 μM (Fig. 1).

Identification of MxiH$^{C\Delta5}$ Residues Interacting with IpaD by NMR Spectroscopy—We used NMR chemical shift mapping to identify the MxiH$^{C\Delta5}$ residues that contact IpaD based on the reasoning that the MxiH$^{C\Delta5}$-IpaD interaction should result in changes in the NMR resonances of MxiH$^{C\Delta5}$. Because the smaller MxiH$^{C\Delta5}$ (8.3 kDa) is more amenable to NMR characterization compared with IpaD, we titrated unlabeled IpaD into ^{15}N-labeled MxiH$^{C\Delta5}$ and monitored the changes in the chemical shifts of MxiH$^{C\Delta5}$ by acquiring several ^{15}N HSQC spectra with increasing amounts of IpaD. Indeed, there are NMR peaks of MxiH$^{C\Delta5}$ that shift upon adding IpaD (Fig. 2). We assigned the resonances of free MxiH$^{C\Delta5}$ using standard three-dimensional NMR experiments (supplemental Fig. S1). Assigning the NMR peaks of free MxiH$^{C\Delta5}$ was challenging because of the broad peaks between 7.8–8.5 ppm in the center of the two-dimensional ^{15}N HSQC spectra (Fig. 2*A*). The narrow proton chemical shift range is consistent with the predominantly α-helical structure of MxiH$^{C\Delta5}$ (15), and the disordered N-terminal 19 residues in the x-ray structure of MxiH$^{C\Delta5}$ (15) likely contribute to the broad peaks between 7.8–8.5 ppm. Nevertheless, using three-dimensional HNCA, CBCA(CO)NH, and

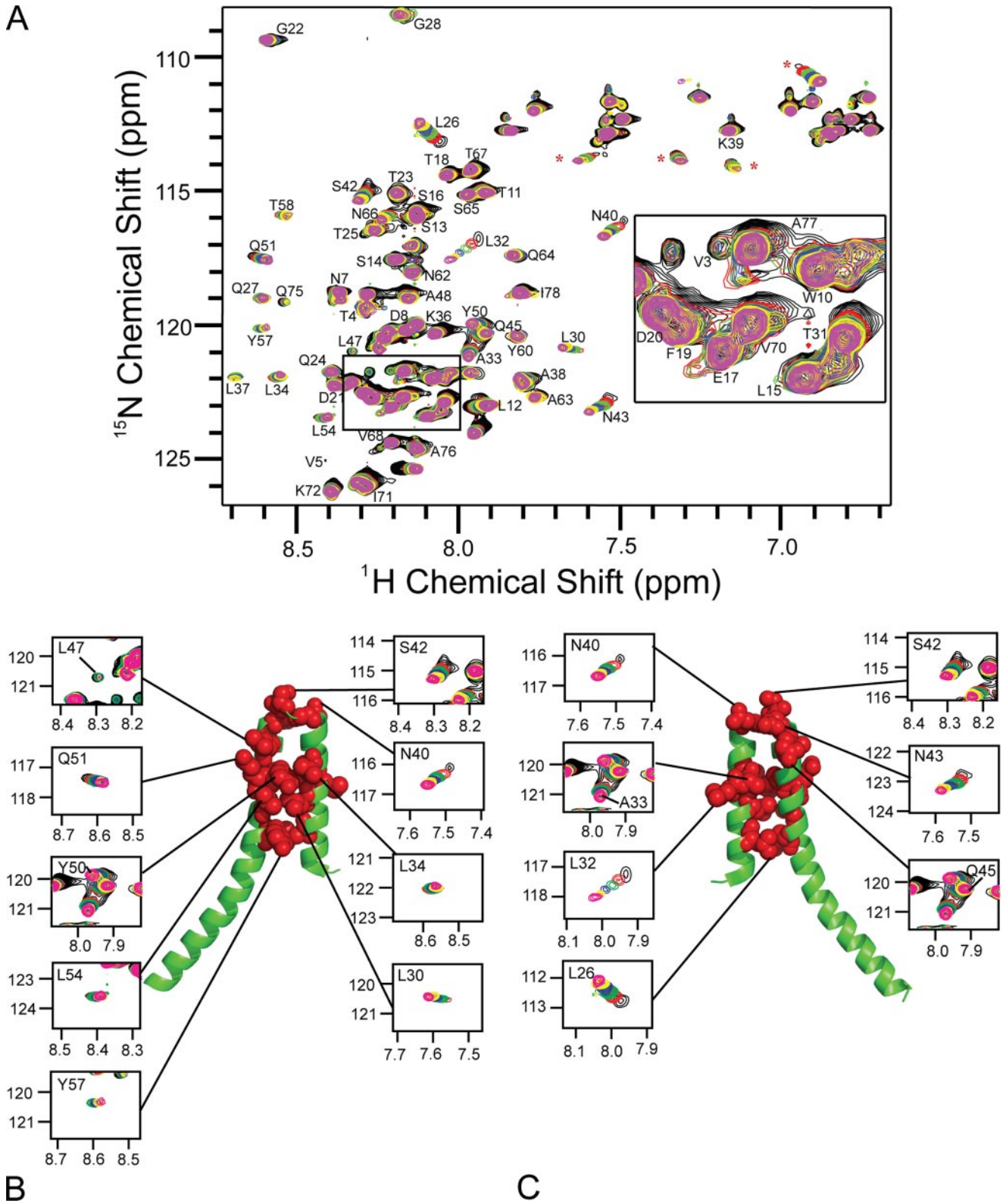

FIGURE 2. *A*, titration of ^{15}N- MxiH$^{C\Delta5}$ with increasing amounts of unlabeled IpaD. Overlay of six protein-nitrogen correlation spectra (^{15}N HSQC) at various MxiH$^{C\Delta5}$:IpaD molar ratios (*black*, 0; *red*, 0.5; *green*, 1.0; *blue*, 2.0; *yellow*, 4.0; *magenta*, 8.0). The actual MxiH$^{C\Delta5}$:IpaD concentrations used are as follows (in μM): *black* (800:0), *red* (320:160), *green* (200:200), *blue* (110:220), *yellow* (60:240), and *magenta* (30:250). Peaks with * could not be assigned because they did not show cross-peaks on the ^{13}C plane in the three-dimensional data sets (HNCA, CBCACONH, and HNCACB) used in the backbone assignments. The *insert* shows an expansion of a crowded region of the ^{15}N HSQC. MxiH$^{C\Delta5}$ contains a single tryptophan, and the side chain Trp-10 N$^{\epsilon1}$ resonance (at ^{15}n = 129.375 and ^{1}H = 10.076) was not perturbed upon addition of IpaD and therefore is not shown. *B*, the HSQC peaks of individual residues affected by IpaD binding are shown separately for clarity. MxiH residues that are perturbed by IpaD are mapped on the surface of the crystal structure of MxiH (Protein Data Bank code 2CA5) (15). *C*, the back side view of *panel B*.

TABLE 1
MxiH mutants used in this study

Mutant protein[a]	Reason for selection[b]	Source
$MxiH^{L34A}$	Minor chemical shift, somewhat conserved	This work
$MxiH^{N40A}$	Major chemical shift, somewhat conserved	This work
$MxiH^{N43A}$	Major chemical shift, conserved	This work
$MxiH^{N43K}$	Same as above, introduces bulky charged group	This work
$MxiH^{L47A}$	Minor chemical shift, highly conserved	This work
$MxiH^{L47D}$	Same as above, introduces charged group	This work
$MxiH^{Y50F}$	Major chemical shift, highly conserved, preserves phenyl ring	This work
$MxiH^{Y50L}$	Same as above, eliminates phenyl ring, preserves hydrophobic side chain	This work
$MxiH^{Q51A}$	Previously shown to retain function and does not interfere with IpaD localization at needle tip	(12,19)

[a] Mutations were introduced into full-length MxiH for complementation analysis using *S. flexneri* SH116. A $MxiH^{C\Delta5}$ version with a C-terminal His_6 was then made for L47A, L47D, Y50F, Y50L, and Q51A for generation of recombinant protein in *E. coli* BL21(DE3). The recombinant protein was used for analyzing interactions with FM-labeled IpaD by fluorescence polarization.
[b] Chemical shifts refer to the NMR shifts described in Fig. 2. Conserved is a measure of the sequence conservation seen among MxiH and its needle protein homologues from *Salmonella typhimurium* (PrgI) and *B. pseudomallei* (BsaL).

HNCACB (supplemental Fig. S1), we assigned 62 of 78 backbone amides of $MxiH^{C\Delta5}$.

Upon adding IpaD to labeled $MxiH^{C\Delta5}$, many $MxiH^{C\Delta5}$ peaks shifted. Further additions of IpaD changed peak positions even more, indicating that binding was in fast exchange NMR time scale. This behavior is consistent with the micromolar binding affinity obtained by fluorescence polarization. The peaks of the PSNP loop residues (Asn-40, Ser-42, Asn-43, and Gln-45) and the head group residues (Leu-26, Leu-30, Leu-32, Ala-33, Leu-34, Tyr-50, Gln-51, Leu-54, and Tyr-57) clearly shifted to a different part of the spectrum (Fig. 2). The latter set of residues form a contiguous surface (Fig. 2, *B* and *C*) when mapped on the x-ray crystal structure of $MxiH^{C\Delta5}$ (15). The side chains of Leu-30, Leu-34, Tyr-50, Gln-51, Leu-54, and Tyr-57 form one face of the contiguous surface (Fig. 2*B*), and the side chains of Leu-26, Leu-32, and Ala-33 are on the "backside" (Fig. 2*C*). Therefore, we propose that the main site of IpaD binding on $MxiH^{C\Delta5}$ is the surface formed by residues in the contiguous surface and the PSNP loop.

In Vivo Analysis of MxiH Mutant Strains—We have also done NMR chemical shift mapping of the MxiH homolog from *Burkholderia pseudomallei*, BsaL, and found that the BsaL residues equivalent to MxiH Leu-30, Leu-54, and Tyr-57 are part of the needle monomer-monomer surface contact.[3] Therefore, we propose that there are two overlapping sites on MxiH: one for IpaD binding and another for MxiH binding and that the Leu-30-Leu-54-Tyr-57 surface (see Fig. 2*B*) is common for both IpaD and MxiH binding. Hence, MxiH mutations were designed to disrupt IpaD binding while maintaining the MxiH-MxiH association. Not all residues that showed chemical shift changes upon IpaD addition were mutated. Gln-51 was previously mutated (see Table 1) and it had no effect on IpaD association with the *Shigella* surface (12, 19). Mutation of Ser-42 was also shown to have no effect on MxiH function (19). Residues that are not conserved among needle proteins from different pathogens were not mutated since the side chain composition at these positions does not appear to be critical. This was the case for Leu-26, Leu-32, Ala-33, and Gln-45 (15, 28). Where NMR assignments were lacking, mutations were not introduced because subsequent interpretation of the data would not be possible. Most importantly, those residues that appeared to have a role in the packing of MxiH monomers[3] were not mutated because the mutations would disrupt needle assembly. Therefore, we did not mutate the MxiH residues (Leu-30, Leu-54, Tyr-57) that appeared to be necessary for MxiH-MxiH contacts. In contrast, Leu-47 showed minor chemical shift changes; however, it is next to the PSNP loop and Tyr-50, and it is invariant among the needle proteins of *Shigella*, *Salmonella*, and *Burkholderia.* In the MxiH structure (15), the side chain of Leu-47 (which is on helix α_2) is oriented toward the surface of the two-helix bundle (Fig. 2*B*). This suggests that Leu-47 is not needed in maintaining the hydrophobic core that dictates the overall fold of the MxiH structure and thus may be involved in IpaD binding. Therefore, Leu-47 was mutated.

Asn-40 and Asn-43 of the MxiH PSNP loop and Leu-34, Leu-47, and Tyr-50 of the contiguous surface were selected for site-specific mutations. Mutations were made to give $MxiH^{L34A}$, $MxiH^{N40A}$, $MxiH^{N43A}$, $MxiH^{N43K}$, $MxiH^{L47A}$, $MxiH^{L47D}$, $MxiH^{Y50F}$, $MxiH^{Y50L}$, and $MxiH^{Q51A}$ (Table 1). For residues Asn-43, Leu-47, and Tyr-50, two substitutions per residue were introduced to explore the importance of side chain composition in needle tip association. $MxiH^{N43A}$ and $MxiH^{N43K}$ were designed to test the impact of replacing a polar residue with either a small nonpolar or a somewhat larger, positively charged residue. $MxiH^{Y50F}$ kept the phenyl ring while $MxiH^{Y50L}$ maintained a hydrophobic side chain. In contrast, the $MxiH^{L47A}$ mutation decreased the length of the hydrophobic side chain while $MxiH^{L47D}$ changed the polarity of the region by adding a negative charge.

The ability of the MxiH mutants to complement the *S. flexneri mxiH* null strain SH116 was assessed using established phenotypic assays with the data summarized in Table 2 (12). First, invasion of Henle 407 cells and contact-mediated hemolysis were used to detect the proper introduction of IpaB/IpaC translocons into targeted cells, which is dependent upon IpaD localization to the TTSA needle tip (10, 12–14). Second, overnight secretion of Ipa proteins provided a measure of functional needle formation. Excessive overnight secretion can provide a measure of the loss of IpaD at the needle tip because *ipaD* null mutants and IpaD mutants that fail to localize at the needle tip are known to be hypersecretive (12, 13, 29). Third, induced (rapid) secretion of Ipa proteins into culture supernatants upon adding Congo red is lost in *ipaD* null mutants and this correlates with the loss of IpaD, but not MxiH, at the bacterial surface (12). In contrast, loss of needle polymerization results in no Ipa

[3] Wang, Y., Picking, W. D., Picking, W. L., and De Guzman, R. N., manuscript in preparation.

TABLE 2
Phenotype of MxiH mutants

Mutant strain[a]	Exposed IpaD/MxiH[b]	Invasion[c]	Hemolysis[d]	Uninduced/induced secretion[e]
Wild type	+/+	100 ± 7[f]	100 ± 14[g]	+/++
mxiH null	−/−	<1 ± 1	2 ± 1	−/−
MxiH$^{C\Delta5}$	−/−	0 ± 0	0 ± 0	−/−
ipaD null	−/+	0 ± 0	0 ± 0	+++/−
MxiH^{L34A}	+/+	44 ± 10	22 ± 5	+/++
MxiH^{N40A}	+/+	82 ± 5	17 ± 3	+/++
MxiH^{N43A}	+/+	77 ± 7	25 ± 3	+/++
MxiH^{N43K}	50%/+	8 ± 3	2 ± 2	++/+
MxiH^{L47A}	−/+	<1 ± 1	2 ± 1	+++/−
MxiH^{L47D}	−/+	<1 ± 1	1 ± 0	+++/−
MxiH^{Y50F}	20%/+	57 ± 8	9 ± 2	++/+
MxiH^{Y50L}	50%/+	51 ± 6	12 ± 2	++/+
[h]MxiH^{Q51A}	+/+	97 ± 8	106 ± 5	++/++

[a] Wild type is pRKMxiH/SH116, the *mxiH* null mutant strain is SH116, and the *ipaD* null mutant is SF622. All other strains are SH116 transformed with the plasmid encoding one of the MxiH point mutants as described here.
[b] Surface localization of IpaD and MxiH was determined by immunofluorescence microscopy. At least 100 bacteria in each of three randomly selected fields were counted (n = 3). In most cases, surface localization was either seen on all bacteria or none in a given field. For some mutants, reduced overall fluorescence was visualized and a reduced number of bacteria were seen with IpaD on their surfaces. In these cases, an approximate percentage of cells having surface IpaD is given.
[c] Invasion is relative to pRKMxiH/SH116 ± S.D. (n = 3).
[d] Contact-mediated hemolysis is relative to pRKMxiH/SH116 ± S.D. (n = 3).
[e] Uninduced secretion is the secretion of TTSS proteins (IpaB and IpaC) into the culture medium during overnight growth. Induced secretion is the secretion of TTSS proteins by bacteria after a 30-min incubation with Congo red (12,19).
[f] Raw value of invasion of Henle cells by pRKMxiH/SH116 is 237 ± 15 colonies.
[g] Raw value of contact-mediated hemolysis of pRKMxiH/SH116 is 2.8 ± 0.02 (A_{545}).
[h] Values are from Ref. 19.

secretion or detection of MxiH on the bacterial surface (12, 14, 19). Thus, if a MxiH mutant fails to maintain IpaD at the needle tip, there will be no invasion, no contact hemolysis, uncontrolled overnight secretion, a loss of Congo red-induced Ipa protein secretion, and no IpaD detected on the bacterial surface (12). Because the MxiH mutants were designed not to interfere with MxiH polymerization, however, MxiH will be detected on the *Shigella* surface and it should be possible to overexpress *mxiH* to form long versions of the TTSA needle that can be sheared from the bacterial surface. The phenotypes of the *mxiH* mutant strains are presented in Table 2.

Asn-40 and Asn-43, which are part of the PSNP loop, were mutated because they showed some of the largest chemical shift perturbations upon addition of IpaD (Fig. 2). Previous results concluded that the polar residues in the PSNP region can tolerate mutation to Ala and still give rise to functional needle tip complexes (19). Similarly, although contact-mediated hemolysis was reduced, N40A and N43A had minimal effects on the phenotypes that measure the needle tip complex formation (Table 2). In contrast, mutation of Asn-43 into the somewhat larger and basic residue Lys decreased needle tip complex formation (Table 2). The decreased ability for this strain to stably maintain IpaD at the needle tip (50% reduction) resulted in lack of secretion control as well as inability to invade Henle 407 cells and lyse erythrocytes (Table 2). Thus, the PSNP loop interacts directly with IpaD and is therefore required for the formation of the MxiH-IpaD tip complex.

Adjacent to the PSNP loop, Leu-34, Leu-47, Tyr-50, and Gln-51 form a contiguous surface on the two-helix bundle and were perturbed upon adding IpaD (Fig. 2*B*). Although the chemical shift of Leu-34 was small, it lies within the contiguous surface, suggesting that Leu-34 could be involved in IpaD binding. Indeed, the L34A mutation partially reduced invasion and hemolysis, suggesting that it has a minor effect on IpaD binding to the needle. Q51A has been characterized (19) and found to have only a partial defect in secretion control, indicating a minor deficiency in IpaD affinity for MxiH.

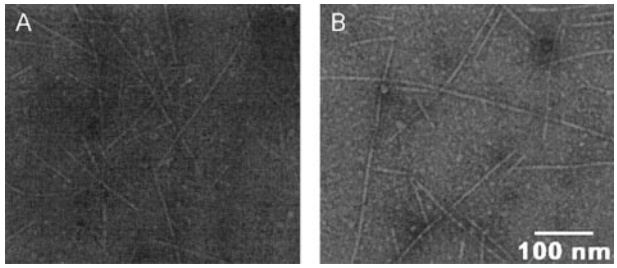

FIGURE 3. **Transmission electron micrographs of sheared needles from *S. flexneri* SH116 expressing MxiH^{L47D} (*A*) or MxiH^{Y50F} (*B*) from a pRK2 plasmid.** Needles were sheared from bacteria in log phase by passage through a 25-gauge needle. The needles were applied to carbon-coated Formvar grids and negatively stained with 2% uranyl acetate.

In contrast to Leu-34 and Gln-51, mutation of Leu-47 and Tyr-50 had significant consequences with regard to *S. flexneri* phenotype and the observed interactions with IpaD *in vitro*. It is also noteworthy that Leu-47 and Tyr-50 are highly conserved among the needle proteins from different species. Both L47A and L47D mutants abolished IpaD surface presentation, resulting in a noninvasive, nonhemolytic strain that also completely lacks secretion control (Table 2). These mutations, however, did not affect MxiH-MxiH interactions since they were capable of needle formation as detected by immunofluorescence microscopy (Table 2) as well as electron microscopy (see Fig. 3*A* for L47D). When recombinant MxiH$^{C\Delta5}$ proteins possessing mutations at Leu-47 were prepared so that their interaction with FM-labeled IpaD could be monitored *in vitro* using FP, a measurable decrease in binding to IpaD was observed (Table 3). Thus, Leu-47 is critical for IpaD-MxiH binding and the proper assembly of IpaD at the needle tip.

Tyr-50 is next to Leu-47 on helix α_2 of MxiH and its phenyl ring forms a network of hydrophobic contacts with residues on helix α_1 that contribute to the stability of the two-helix bundle (15). The hydroxyl group of Tyr-50, however, is pointed toward the MxiH surface and is not involved in any intramolecular contacts (15). Therefore, the Tyr-50 hydroxyl group is not

required in stabilizing the overall fold of the two-helix bundle. Structurally, a phenylalanine or leucine in this position would be expected to maintain the hydrophobic core and the overall fold of the two-helix bundle, yet Tyr-50 is invariant among the needle proteins of *Shigella*, *Salmonella*, and *Burkholderia*. Thus, the mutations Y50F and Y50L were made and the phenotypes of each mutant strain determined (Table 2). Although not as severe as the Leu-47 mutations, Y50L and Y50F resulted in a 50–80% reduction in IpaD surface presentation, which negatively affects invasion, hemolysis, or secretion control (Table 2). Our data, however, show that both Y50F and Y50L form stable needles *in vivo* when examined by either immunofluorescence (Table 2) or electron microscopy (Fig. 3). As with Leu-47, the recombinant MxiH$^{C\Delta5}$ proteins possessing the Tyr-50 mutations were purified to examine their binding interaction with FM-labeled IpaD. Indeed, like the Leu-47 mutants, the Tyr-50 mutants have a notable increase in the apparent dissociation constant, with Y50F being 3-fold higher and Y50L being 5-fold higher (Table 3). Thus, although the hydroxyl group has a role in the stable maintenance of IpaD at the TTSA needle tip, the hydrophobic interactions through the phenyl ring appear to contribute more to the *in vitro* interaction between IpaD and MxiH$^{C\Delta5}$. Taken together, the data indicate that key residues of the contiguous face and those of the PNSP loop contribute to the proper binding, maintenance, and function of the MxiH-IpaD tip complex (Fig. 4).

TABLE 3

Association of MxiH mutant proteins with FM-IpaD by fluorescence polarization

ND, not determined.

Mutant protein	Maximum observed ΔmP[a]	Apparent dissociation constant[b]
Wild type	24.6 ± 2.0	0.48
MxiH^{L47A}	7.8 ± 0.7	2.47
MxiH^{L47D}	−1.7 ± 0.9	ND
MxiH^{Y50F}	7.6 ± 0.4	1.30
MxiH^{Y50L}	12.8 ± 0.8	2.48
MxiH^{Q51A}	24.7 ± 0.9	0.65

[a] The change in polarization is presented in millipolarization units.
[b] The apparent dissociation constant was determined using 25 nM FM-IpaD using Sigmaplot®.

Previously, we have shown that the C-terminal coil of IpaD is required for its association with the MxiH needle and that the N-terminal globular domain is external to the needle (12). Modeling using the recently solved individual crystal structures of MxiH and IpaD, however, was unable to explain how IpaD docks atop the MxiH needle other than that the orientation is likely to be the same as that predicted for LcrV (15, 16, 30). Based on their crystal structures, Johnson *et al.* (16) proposed a model for the interaction of MxiH with IpaD based on the fact that the IpaD N-terminal domain is structurally similar to MxiH and therefore could serve as a cytoplasmic intramolecular chaperone that prevents the interaction of IpaD with MxiH prior to recruitment of the IpaD to the bacterial surface. The IpaD N-terminal helices H1 and H2 pack together in such a way that the MxiH structure can be superimposed on the MxiH two-helix bundle (α_1 and α_2) with a C$^\alpha$ root mean square deviation of 3.2 Å (Fig. 4, *left*). This structural similarity is quite striking considering that the C$^\alpha$ root mean square deviation between the two needle homologs BsaL and MxiH is also 3.2 Å (28). This suggests that IpaD has a built-in surface that complements the size and shape of that portion of MxiH that is responsible for maintaining IpaD at the TTSA needle tip. Our NMR chemical shift-mapping results provide the first biological data to support such a model in that the MxiH residues that are perturbed upon adding IpaD appear to form a contiguous face (Fig. 4, *right*) that may actually be contacting a yet unidentified surface on IpaD and this interaction is blocked in the bacterial cytoplasm by the presence of the IpaD N terminus. MxiH residues within the region capable of interacting with IpaD would include the side chains of Leu-47 and Tyr-50, which upon mutation in this study abolished or severely perturbed IpaD localization. Furthermore, in this model, the MxiH PSNP loop would directly abut helices H3 and H7 of IpaD and such an interaction would be sterically impossible based upon the crystal structure of full-length IpaD unless the N-terminal domain were moved away upon tip complex assembly. Indeed, the chemical

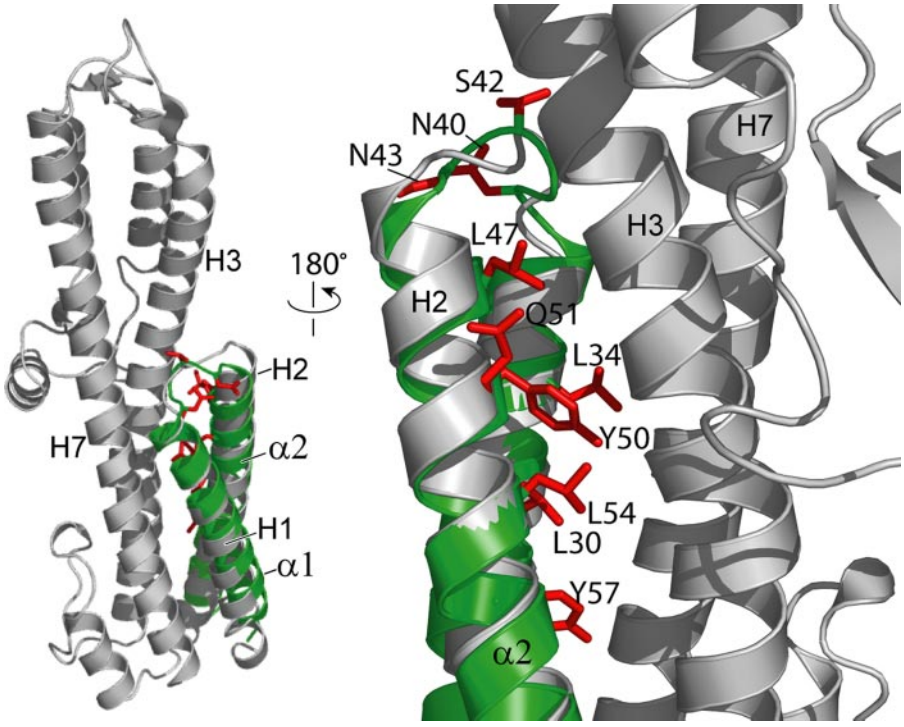

FIGURE 4. **Model of MxiH-IpaD binding.** *Left*, the two-helix bundle of MxiH (*green*, α_1 and α_2) can be superimposed with helices H1 and H2 of IpaD (*gray*) with a C$^\alpha$ root mean square deviation of 3.2 Å. *Right*, the MxiH-IpaD binding interface is expanded, and the figure is rotated by 180° relative to the orientation in *panel A*. The side chains of MxiH residues (Leu-30, Leu-34, Tyr-50, Leu-54, Tyr-57) that showed NMR chemical shift perturbation upon titration of IpaD as well as Leu-47 are all oriented toward helices H3 and H7 of IpaD. The loop residues (Asn-40, Ser-42, and Asn-43, *red*) also showed chemical shift perturbations.

shifts of Asn-40, Ser-42, and Asn-43 demonstrate an interaction between the PSNP loop and IpaD does exist, suggesting that it is possible that the N-terminal domain moves away upon tip complex assembly. Unfortunately, at this time we are unable to predict how the N terminus (helix H1-H2′) "swings away" during tip complex assembly to permit docking atop the MxiH needle. Because it has been postulated that the needle channel cannot accommodate a fully folded IpaD (15, 31), it is possible that it travels through the needle channel in a partially unfolded manner (31, 32) and that refolding at the needle tip forces it to assume a conformation that is compatible with the MxiH-IpaD interactions demonstrated here.

High resolution structures are also available for the MxiH/IpaD counterparts in *B. pseudomallei*, BsaL/BipD, and a similar BsaL-BipD binding model can be generated in which the two-helix bundle of BsaL can be superimposed to the N-terminal helices of BipD, also with a C^{α} root mean square deviation of 3.2 Å (data not shown). We have also completed the NMR structure of PrgI (28) and shown that it is structurally homologous to MxiH and BsaL. The homology of SipD with BipD and IpaD suggests similarities in the structure of SipD. This suggests that the model of MxiH-IpaD or BsaL-BipD interaction might be a common feature of needle tip interaction for *Shigella*, *Salmonella*, and *Burkholderia*.

Acknowledgments—Critical reading of the manuscript by R. Kenjale, C. R. Middaugh, and members of the Picking and De Guzman groups is acknowledged.

REFERENCES

1. Mohle-Boetani, J. C., Stapleton, M., Finger, R., Bean, N. H., Poundstone, J., Blake, P. A., and Griffin, P. M. (1995) *Am. J. Public Health* **85,** 812–816
2. Dutta, S., Ghosh, A., Ghosh, K., Dutta, D., Bhattacharya, S. K., Nair, G. B., and Yoshida, S. (2003) *J. Clin. Microbiol.* **41,** 5833–5834
3. Parsot, C., and Sansonetti, P. J. (1996) *Curr. Top. Microbiol. Immunol.* **209,** 25–42
4. Zychlinsky, A., Prevost, M. C., and Sansonetti, P. J. (1992) *Nature* **358,** 167–169
5. Tran Van Nhieu, G., and Sansonetti, P. J. (1999) *Curr. Opin. Microbiol.* **2,** 51–55
6. Cossart, P., and Sansonetti, P. J. (2004) *Science* **304,** 242–248
7. Buttner, D., and Bonas, U. (2002) *Trends Microbiol.* **10,** 186–192
8. He, S. Y., Nomura, K., and Whittam, T. S. (2004) *Biochim. Biophys. Acta* **1694,** 181–206
9. Kubori, T., Matsushima, Y., Nakamura, D., Uralil, J., Lara-Tejero, M., Sukhan, A., Galan, J. E., and Aizawa, S. I. (1998) *Science* **280,** 602–605
10. Blocker, A., Jouihri, N., Larquet, E., Gounon, P., Ebel, F., Parsot, C., Sansonetti, P., and Allaoui, A. (2001) *Mol. Microbiol.* **39,** 652–663
11. Cordes, F. S., Komoriya, K., Larquet, E., Yang, S., Egelman, E. H., Blocker, A., and Lea, S. M. (2003) *J. Biol. Chem.* **278,** 17103–17107
12. Espina, M., Olive, A. J., Kenjale, R., Moore, D. S., Ausar, S. F., Kaminski, R. W., Oaks, E. V., Middaugh, C. R., Picking, W. D., and Picking, W. L. (2006) *Infect. Immun.* **74,** 4391–4400
13. Picking, W. L., Nishioka, H., Hearn, P. D., Baxter, M. A., Harrington, A. T., Blocker, A., and Picking, W. D. (2005) *Infect. Immun.* **73,** 1432–1440
14. Olive, A. J., Kenjale, R., Espina, M., Moore, D. S., Picking, W. L., and Picking, W. D. (2007) *Infect. Immun.* **75,** 2626–2629
15. Deane, J. E., Roversi, P., Cordes, F. S., Johnson, S., Kenjale, R., Daniell, S., Booy, F., Picking, W. D., Picking, W. L., Blocker, A. J., and Lea, S. M. (2006) *Proc. Natl. Acad. Sci. U. S. A.* **103,** 12529–12533
16. Johnson, S., Roversi, P., Espina, M., Olive, A., Deane, J. E., Birket, S., Field, T., Picking, W. D., Blocker, A. J., Galyov, E. E., Picking, W. L., and Lea, S. M. (2007) *J. Biol. Chem.* **282,** 4035–4044
17. Espina, M., Ausar, S. F., Middaugh, C. R., Baxter, M. A., Picking, W. D., and Picking, W. L. (2007) *Protein Sci.* **16,** 704–714
18. Marquart, M. E., Picking, W. L., and Picking, W. D. (1995) *Biochem. Biophys. Res. Commun.* **214,** 963–970
19. Kenjale, R., Wilson, J., Zenk, S. F., Saurya, S., Picking, W. L., Picking, W. D., and Blocker, A. (2005) *J. Biol. Chem.* **280,** 42929–42937
20. Deane, J. E., Cordes, F. S., Roversi, P., Johnson, S., Kenjale, R., Picking, W. D., Picking, W. L., Lea, S. M., and Blocker, A. (2006) *Acta Crystallogr. Sect. F Struct. Biol. Crystallogr. Commun.* **62,** Pt. 3, 302–305
21. Zhang, L., Wang, Y., Picking, W. L., Picking, W. D., and De Guzman, R. N. (2006) *J. Mol. Biol.* **359,** 322–330
22. Darboe, N., Kenjale, R., Picking, W. L., Picking, W. D., and Middaugh, C. R. (2006) *Protein Sci.* **15,** 543–552
23. Delaglio, F., S. Grzesiek, G. W. Vuister, Z. Guang, J. Pfeifer, and Bax, A. (1995) *J. Biomol. NMR* **6,** 277–293
24. Johnson, B. A., and Blevins, R. A. (1994) *J. Biomol. NMR* **4,** 604–613
25. Picking, W. L., Coye, L., Osiecki, J. C., Barnoski Serfis, A., Schaper, E., and Picking, W. D. (2001) *Mol. Microbiol.* **39,** 100–111
26. Bahrani, F. K., Sansonetti, P. J., and Parsot, C. (1997) *Infect. Immun.* **65,** 4005–4010
27. Harrington, A. T., Hearn, P. D., Picking, W. L., Barker, J. R., Wessel, A., and Picking, W. D. (2003) *Infect. Immun.* **71,** 1255–1264
28. Wang, Y., Ouellette, A. N., Egan, C. W., Rathinavelan, T., Im, W., and De Guzman, R. N. (2007) *J. Mol. Biol.* **371,** 1304–1314
29. Menard, R., Sansonetti, P., and Parsot, C. (1994) *EMBO J.* **13,** 5293–5302
30. Mueller, C. A., Broz, P., Muller, S. A., Ringler, P., Erne-Brand, F., Sorg, I., Kuhn, M., Engel, A., and Cornelis, G. R. (2005) *Science* **310,** 674–676
31. Erskine, P. T., Knight, M. J., Ruaux, A., Mikolajek, H., Sang, N. W., Withers, J., Gill, R., Wood, S. P., Wood, M., Fox, G. C., and Cooper, J. B. (2006) *J. Mol. Biol.* **363,** 125–136
32. Akeda, Y., and Galan, J. E. (2005) *Nature* **437,** 911–915

Supplementary material.

IDENTIFICATION OF THE MxiH NEEDLE PROTEIN RESIDUES RESPONSIBLE FOR ANCHORING IpaD TO THE TYPE III SECRETION NEEDLE TIP

Lingling Zhang, Yu Wang, Andrew J. Olive, Nathan D. Smith, William D. Picking, Roberto N. De Guzman, Wendy L. Picking

From the Department of Molecular Biosciences, University of Kansas, Lawrence, KS 66045

The primers used to make the plasmid constructs encoding the mutant proteins are described below (plasmid, mutant protein with primers listed below)

pLZL34A **MxiH^{L34A}**

5’ GAGAGAGAGAACGTTGGCA*GCA*GATAAATTAGCTAAAAATCCT

5’ GAGAGAGAGAACGTTAGTTCACCTTGTAATGT

pLZN40A **MxiH^{N40A}**

5’ GAGAGAGAGTTCGAAGG*AGC*TTTAGCTAATTTATCTAGTGC

5’ GAGAGAGAGTTCGAATCCACAGTTGCTGGCTG

pLZN43A **MxiH^{N43A}**

5’ GAGAGAGAGCAATTGTGG*TGC*CGAAGGATTTTTAGCTAATTT

5’ GAGAGAGAGCAATTGCTGGCTGAATACCAAA

pLZN43K **MxiH^{N43K}**

5’ GAGAGAGAGCAATTGTGG*TTT*CGAAGGATTTTTAGCTAATTT

5’ GAGAGAGAGCAATTGCTGGCTGAATACCAAA

pLZL47A **MxiH^{L47A}**

5’ GAGAGAGAGCAATTG*GCT*GCTGAATACCAAAGTAAATTA

5’ GAGAGAGAGCAATTGTGGATTCGAAGGATTTT

pLZL47D MxiH^{L47D}

5’ GAGAGAGAGCAATTG*GAT*GCTGAATACCAAAGTAAATTA

5’ GAGAGAGAGCAATTGTGGATTCGAAGGATTTT

pLZY50F MxiH^{Y50F}

5’ GAGAGAGAGCAATTGCTGGCTGAA*TTT*CAAAGTAAATTATCTGAATAT

5’ GAGAGAGAGCAATTGTGGATTCGAAGGATTTT

pLZY50L MxiH^{Y50L}

5’ GAGAGAGAGCAATTGCTGGCTGAA*CTG*CAAAGTAAATTATCTGAATAT

5’ GAGAGAGAGCAATTGTGGATTCGAAGGATTTT

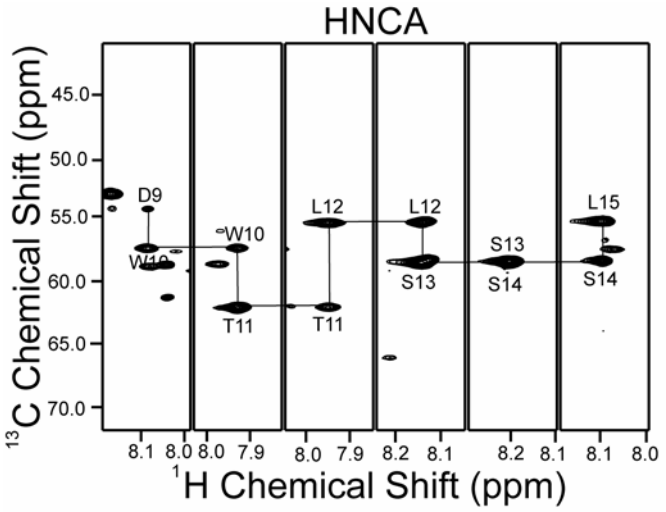

Supplemental Figure 1. Portion of the 3D HNCA spectra of ^{15}N,^{13}C-MxiH $^{C\Delta5}$, shown as ^{13}C,^{1}H strips (the ^{15}N chemical shift is on the Z-axis), for residues W10-L15. Each strip shows the Cα of the current residue and the Cα of the preceding residue, in an HNCA walk or connectivity. The HNCA data, together with CBCA(CO)NH and HNCACB data, confirms the backbone assignments for W10-L15. The backbone assignments for the rest of the protein were obtained in a similar manner. HNCA spectra were acquired using a 0.8 mM ^{15}N,^{13}C-MxiH $^{C\Delta5}$ sample at 800 MHz and 25°C.

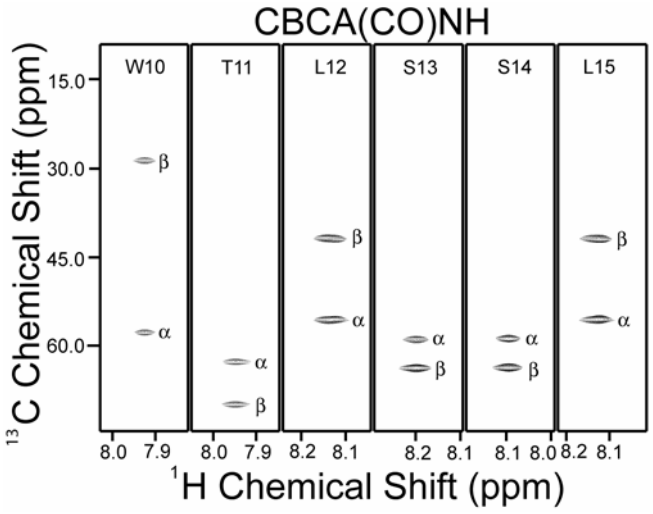

Supplementary Figure 2. Portion of the 3D CBCA(CO)NH spectra of ^{15}N,^{13}C-MxiH$^{C\Delta5}$ shown as ^{13}C,^{1}H strips for W10 to L15 (the ^{15}N ppm is on the Z-axis). The CBCA(CO)NH experiment shows unambiguously the Cα and Cβ of the preceeding residue together with backbone amide (^{1}H and ^{15}N) of the current residue. The CBCA(CO)NH data is used together with HNCA and HNCACB to assign the backbone resonances of free MxiH$^{C\Delta5}$. The spectra were acquired using a 0.8 mM ^{15}N,^{13}C-MxiH $^{C\Delta5}$ sample at 800 MHz and 25°C.

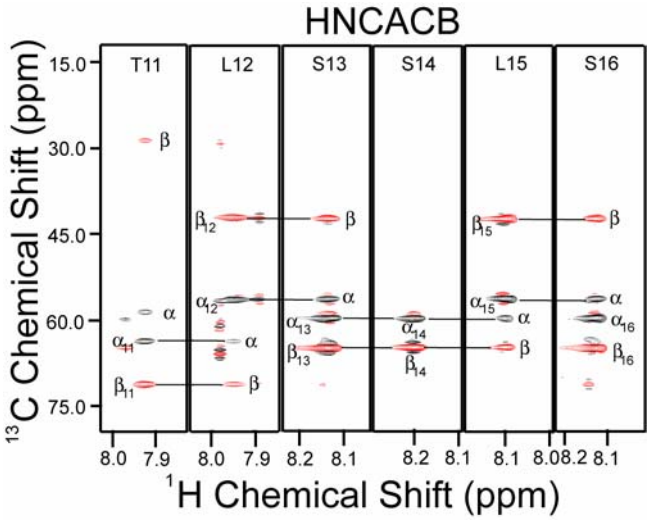

Supplementary Figure 3. Portion of the 3D HNCACB spectra of ^{15}N,^{13}C-MxiH$^{C\Delta5}$, shown as ^{13}C,^{1}H strips for T11-S16 (the ^{15}N ppm is on the Z-axis). Each strip shows the Cα and Cβ of the preceeding and current residue and the amide (^{1}H and ^{15}N) resonances of the current residue. The Cα and Cβ have opposite phases (shown as black and red peaks). In theory, the 3D HNCACB dataset contains all the information needed in assigning all the backbone resonances of a protein. However, this experiment is insensitive, and was used in combination with the more sensitive HNCA and CBCA(CO)NH experiments to complete the backbone assignments of free MxiH$^{C\Delta5}$. The spectra were acquired using a 0.8 mM ^{15}N,^{13}C-MxiH $^{C\Delta5}$ sample at 800 MHz and 25°C.

Identification of the MxiH Needle Protein Residues Responsible for Anchoring Invasion Plasmid Antigen D to the Type III Secretion Needle Tip

Lingling Zhang, Yu Wang, Andrew J. Olive, Nathan D. Smith, William D. Picking, Roberto N. De Guzman and Wendy L. Picking

J. Biol. Chem. 2007, 282:32144-32151.
doi: 10.1074/jbc.M703403200 originally published online September 7, 2007
